Available online at www.sciencedirect.com
SCIENCE DIRECT®
Journal of volcanology and geothermal research
ELSEVIER
Journal of Volcanology and Geothermal Research 144 (2005) 119–136
www.elsevier.com/locate/jvolgeores

Elliptical calderas in active tectonic settings: an experimental approach

E.P. Holohan[a], V.R. Troll[a,*], T.R. Walter[b], S. Münn[c], S. McDonnell[a], Z.K. Shipton[a,d]

[a]*Trinity College, Dept. of Geology, Dublin 2, Ireland*
[b]*MGG/RSMAS, University of Miami, FL 33149, USA*
[c]*GEOMAR, Dept. of Volcanology and Petrology, 24148 Kiel, Germany*
[d]*Centre for Geosciences, University of Glasgow, Lilybank Gardens, Glasgow G12 8QQ, Scotland, UK*

Received 16 November 2004; accepted 16 November 2004

Abstract

Caldera volcanoes form due to collapse of a magma chamber roof into the underlying magma chamber. Many field, theoretical and experimental studies have postulated that calderas are delimited by reverse ring faults and are surrounded by peripheral concentric normal faults. In the simplest theoretical scenario, circular magma chambers produce circular calderas. Many calderas, however, are elliptical in shape, particularly those in extensional and compressive tectonic settings. Several factors may explain elliptical calderas. The first is the presence of an elliptical magma chamber, established by, for instance, preferential intrusion along pre-existing basement structures or differential spalling of the magma chamber walls. The second is the overlap (nesting) of several discrete calderas to form a single, larger elliptical structure. The third is asymmetric subsidence. The fourth is variable pre-collapse topography. A fifth possible factor is distortion of the caldera faults by the regional stress field during caldera formation. A sixth factor is the post-collapse distortion of the caldera structure due to continued regional deformation.

To better understand relationships between caldera surface expression, reservoir geometry and regional tectonic stresses, we conducted scaled analogue experiments. These experiments examined the impact of regional stress and associated structures on calderas formed during evacuation of reservoirs (circular rubber balloons) of known dimensions and depths. The results show that, in principle, calderas produced in compression/extension experiments are elongated parallel to the direction of minimum horizontal compressive stress, despite the chamber beneath being circular in plan view. As a consequence, model ring fault orientation varied from steeply dipping where striking perpendicular to the minimum horizontal regional compressive stress, to shallower dips where striking parallel to the minimum horizontal regional compressive stress. This leads us to suggest that the influence of a regional stress field on caldera fault orientation during and/or after caldera formation may be significant in the development of elliptical calderas. In addition, such variation of caldera ring fault dip from steep to relatively shallow could influence location and behaviour of ring fissure eruptions.

Keywords: collapse calderas; volcano tectonics; ring faults; analogue modeling; elliptical calderas

* Corresponding author. Fax: +353 1 671 1199.
E-mail address: trollv@tcd.ie (V.R. Troll).

0377-0273/$ - see front matter © 2004 Elsevier B.V. All rights reserved.
doi:10.1016/j.jvolgeores.2004.11.020

1. Introduction

1.1. The elliptical caldera problem

Calderas are kilometer-scale volcanic depressions that form due to collapse of a magma chamber roof into the underlying magma body (Anderson, 1936; Smith and Bailey, 1968; Lipman, 1997). The structural characteristics and subsidence mechanisms of calderas have long been a subject of debate (see McBirney, 1990; Lipman, 1997 for reviews). This is because exposure of structures at many caldera complexes is limited. Calderas are frequently infilled by pyroclastic and epiclastic debris, blanketed by thick layers of ash-flow deposits and/or obscured by post-caldera intrusions. In recent years, analogue modeling experiments simulating caldera formation have been conducted to surmount such difficulties. These experiments have focused on examining the structural effects of local volcano-tectonic stresses generated by doming (or resurgence), due to a rising or expanding magma body, and/or collapse, from magma chamber evacuation and deflation (Komuro et al., 1984; Komuro, 1987; Marti et al., 1994; Acocella et al., 2000; Roche et al., 2000; Roche and Druitt, 2001; Walter and Troll, 2001; Troll et al., 2002; Cailleau et al., 2003).

These analogue studies, as well as analytical and numerical approaches (e.g., Gudmundsson, 1988; Gudmundsson et al., 1997), demonstrate that magma chambers that are circular in plan view and do not experience far-field stresses produce calderas and domes that are also of circular surface expression. In nature, however, many calderas are elliptical in shape and lie in extensional and compressive regional tectonic settings (Table 1), a combination of facts that has received relatively little attention in the literature. Indeed, many of the classic type-locality calderas, such as Valles (New Mexico, USA), Long Valley (California, USA), Yellowstone (Wyoming, USA), Krakatau (Sunda Strait, Indonesia), Santorini (Cyclades, Greece) and Cerro Galan (Puna, Argentina) are noticeably elliptical in plan view. Elliptical calderas are also found on other planets, such as Uranius Patera on Mars (Miller, 2001).

Table 1
Examples of elliptical calderas in varying tectonic settings

Caldera	Location	Tectonic setting	Long axis (km)	Short axis (km)	Ω	β	Data source(s)
Katmai	Aleutian Arc, Alaska	Compressional	4	2.5	0	90	Wallmann et al., 1990; Hildreth and Fierstein, 2000
Suswa	Kenyan Rift Valley	Extensional	11.3	8.6	0	90	Skilling, 1993; Bosworth et al., 2000
Taupo (Oruanui)	TVZ, New Zealand	Extensional	27.6	14.5	0	90	Wilson et al., 1995; Acocella et al., 2003
Cerro Galan	Central Andes (NW Argentina)	Transpressional (?)	34	20	0	0	Francis et al., 1978; Marrett et al., 1994
Valles	Rio Grande Rift, New Mexico	Transtensional	17.2	12.5	0	70	J. Wolff, 2003 (pers. comm.); Aldrich et al., 1986
Long Valley	Basin and Range, California	Transtensional	20.4	8	0	65	Moos and Zoback, 1993; Bosworth et al., 2003
Campi Flegrei	Campanian Plain, Italy	Transtensional	17.1	11.5	5	30	Orsi et al., 1996; Bianco et al., 1998
Gariboldi	Ethiopian Rift valley	Transtensional	7.5	5	34±20	16±20	Acocella et al., 2002
Gedemsa	Ethiopian Rift Valley	Transtensional	9	7	34±9	18±9	Acocella et al., 2002
Kapenga	TPZ, New Zealand	Transtensional	27.4	14.8	85	0	Wilson et al., 1995; Acocella et al., 2003

Tectonic regime quoted is that at time of formation as can best be reconstructed. Ω is the acute angle between the caldera's long axis and the regional least horizontal compressive stress. β is the acute angle between the caldera's long axis and the main regional fault trend. TVZ—Taupo Volcanic Zone.

A number of factors may possibly explain why calderas have an elliptical surface expression. These include:

1) A horizontally elongated magma body due to regional stresses in the crust. One possible mechanism to create such a body is preferential lateral growth along crustal anisotropies such as pre-existing or syn-tectonic fault trends (cf. Acocella et al., 2002). Alternatively, a mechanism analogous to borehole breakout, whereby regional stresses cause differential spalling of a magma chamber's walls, may also lead to lateral elongation of a magma chamber (Bosworth et al., 2003).
2) Overlap of several collapse structures, each of which is related to an individual collapse event and possibly also associated with a discrete magma chamber. The overlapping collapse structures form a composite or 'nested' caldera structure with elongate geometry (cf. Marti et al., 1994).
3) Asymmetric subsidence can give rise to a caldera with an elliptical plan view outline, even if the underlying magma chamber is circular (Kennedy et al., 2004).
4) Pre-collapse topography exerts control on the plan view surface expression of the caldera structure by determining which levels caldera faults intersect the surface (Walter and Troll, 2001; Belousov et al., 2004). It may also cause a variable loading distribution across the magma chamber roof, which affects ring fault geometries (Walter and Troll, 2001) and promotes asymmetric subsidence (Lavallée et al., 2004).
5) A 'distortion' of caldera faults due to interaction of volcanic and regional stress fields during caldera formation.
6) A distortion of the caldera structure due to progressive post-collapse regional deformation.

The first factor outlined assumes that the elliptical shape of a caldera more or less directly reflects the plan view geometry of the underlying magma chamber (cf. Gudmundsson, 1988; Newhall and Dzurisin, 1988; Roche et al., 2000). Implicit in the last four factors is that the plan view shape of the caldera deviates significantly from that of the underlying magma reservoir. With regard to the second factor, nesting, it is conceivable that both magma chamber elongation, syn-collapse 'fault distortion' and topography may each play a role in the formation of an overlapping nested caldera structure.

The aim of this study is to investigate the effects of far-field (i.e., regional tectonic) stresses and related structures on caldera development and its associated near-field structural patterns. Focusing on the fifth factor, we conducted scaled analogue experiments in order to examine its possible influence. Our experiments concentrated on structures formed during evacuation and deflation of a magma reservoir, under orthogonal (i.e., no strike slip) extensional and compressive tectonic regimes.

1.2. Previous work

The recent experimental and theoretical studies cited above show that calderas can form either as a result of crustal doming due to inflation of a magma chamber or, conversely, by crustal down-warp due to magma chamber deflation. Pre-caldera doming or post-caldera resurgence due to inflation of a magma chamber generates a structural pattern consisting of mainly radial and subordinate concentric fractures. Radial fractures are extensional and propagate outwards from the center of the dome. Associated concentric fractures are initially inward-dipping reverse faults (cf. Walter and Troll, 2001). High tensional stresses at the dome apex may result in their reactivation with a normal displacement. Small-scale caldera formation (apical graben) could occur as a result of such down faulting at the dome apex (Komuro, 1987; Troll et al., 2000). Analytical and numerical studies (Gudmundsson, 1988, 1998; Gudmundsson et al., 1997) indicate that larger scale regional doming, in combination with magma chamber overpressure, can concentrate tensional and normal stresses above the margins of magma chambers, leading to similar normal fault caldera formation.

In calderas formed by deflation of a magma chamber (withdrawal of magmatic support), the subsiding rock mass is most likely accommodated along concentric, vertical to outward-dipping ('bell-shaped') reverse faults (Anderson, 1936; Komuro,

1987; Branney, 1995; Roche et al., 2000; Acocella et al., 2000; Walter and Troll, 2001). No radial faults form during such collapse. A concentric zone of extension forms peripheral to the subsiding caldera center and is accommodated by the formation of vertical to inward-dipping normal faults. When preceded by a doming phase, collapse due to deflation results in closure of radial fractures, with possible inverted reactivation of the inward-dipping faults of the doming phase (Troll et al., 2002).

As shown in Fig. 1, a caldera forming due to deflation of the underlying reservoir can be divided into two generalized structural zones:

1) The *intracaldera* is the main area of subsidence and is structurally delimited by the outermost reverse ring fault. The collapse of the chamber roof can be accommodated by the sequential development of several reverse ring faults. Based on previous analogue experiments, the main displacement typically occurs on a reverse ring fault connected to the margins of the magma chamber (Roche et al., 2000).
2) The *peripheral fault zone* is the area extending outward from the main reverse ring fault to the outermost caldera-associated concentric faults. The peripheral zone is characterized by extension, 'downsag' and normal faulting (cf. Branney, 1995; Walter and Troll, 2001).

Together, these two zones comprise the total structural and morphological expression of a collapse caldera.

2. Experimental set-up and procedure

2.1. Experimental apparatus

The experimental apparatus (Fig. 2) consisted of a sand-filled box with two free walls (end walls), similar to that used by Mandl (1987) and Cailleau et al. (2003). Inward and outward motions of the end walls respectively exerted horizontal compressive stress and horizontal extensional stress on the sand medium, approximating pure shear strain in both cases. A rubber sheet beneath the sand pile was securely fixed to the bottom of the end walls only. When the end walls moved apart, the basal rubber sheet was stretched and distributed the regional stresses uniformly across the deforming medium (as evidenced by an even distribution of consistently spaced faults). Sill-like rubber balloons buried in the sand were used to simulate magma chambers in the brittle crust. These balloons were circular in plan view and had rigid rims to preserve their plan view shape when under stress. The balloons were inflated and deflated via a narrow tube connected to an air inlet valve outside the sandbox.

2.2. Scaling and material properties

Two end-member analogue materials, sand and wheat flour, were used in the experiments to simulate brittle deformation of the crust (see Walter and Troll, 2001 for more detailed description). We used sieved (mean grain diameter ~300 μm) dry, aeolian quartz

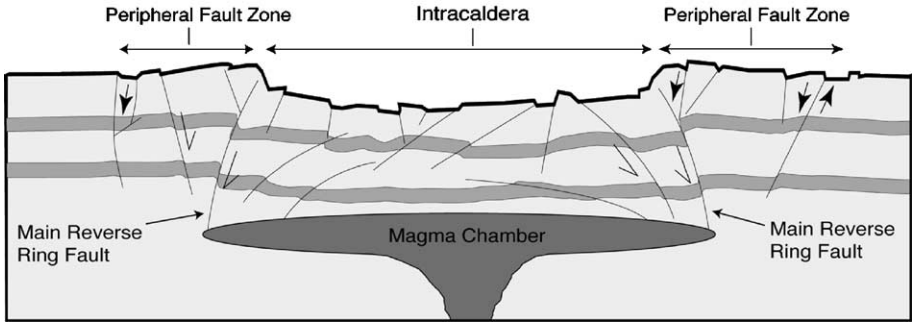

Fig. 1. Schematic cross section through a collapse caldera based on structures produced during analogue modelling of magma chamber deflation in the absence of tectonic stress (Walter and Troll, 2001). The peripheral zone and the intracaldera together comprise the total morphological expression of a caldera.

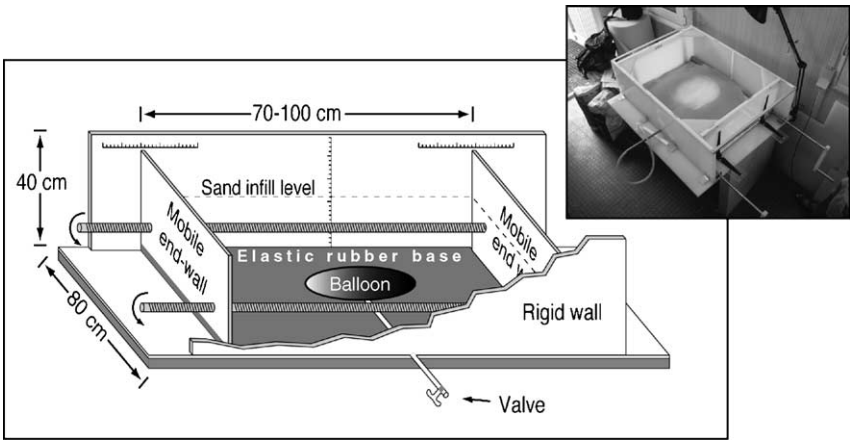

Fig. 2. Photograph and technical sketch of the experimental set-up. Turning the handles moved the end walls inward/outward, simulating regional forces of compression/extension respectively. The rubber balloons were sill-like with rigid rims to preserve plan view circular shape. A basal rubber sheet maintained a uniform stress distribution across the deforming medium.

sand, with a bulk density (ρ_S) of 1300–1500 kgm^{-3} and dry flour (mean grain diameter of 100–200 μm) with a bulk density (ρ_F) of 570 kgm^{-3}. Combinations of sand and flour (mixed respectively in ratios of 3:1 and 12:1 by weight) with corresponding bulk densities (ρ_{SF}) of 1400 and 1200 kgm^{-3} were also used as intermediates between the two end-member materials. The density range for natural rocks is approximately 2000–3300 kgm^{-3}, with most rocks (granites, basalts, hard limestones etc.) lying between 2600 and 3000 kgm^{-3} (Goodman, 1989).

Material properties and forces in the experiments should obey the principle of geometric and dynamic similarity (Hubbert, 1951) and operate according to a consistent scaling ratio (X^*), determined by $X^*=X_{Model}/X_{Nature}$ (see also Roche et al., 2000). The geometric scaling factor (length ratio, $l^*=l_{Model}/l_{Nature}$) was approximately 10^{-5}, so that 1 cm in the model corresponds to ~1 km in nature. The dynamic scaling factor (stress ratio, $\sigma^*=\sigma_{Model}/\sigma_{Nature}$) is calculated from the equation $\sigma^*=\rho^*g^*l^*$. As the densities of the analogue materials are less than natural rocks by a factor of approximately 2 (i.e., $\rho^*=0.5$) and gravitational acceleration is the same in both model and nature (i.e., $g^*=1$), the required stress ratio for a geometric scaling factor of 10^{-5} was $\sigma^*=5\times10^{-6}$.

Dry, medium-grained sand obeys a straight-line Mohr–Coulomb failure criterion, which is also assumed to apply to rocks in the brittle crust (Hubbert, 1951). Cohesion of natural rocks lies in the range of 10^5–10^7 Pa, which when scaled down by 5×10^{-6}, gives a required cohesion of 0.5–50 Pa for the analogue materials. Both analogue materials were subjected to direct shear tests to find their angles of internal friction (ϕ) and cohesion (C—Walter and Troll, 2001). The cohesion for sand used was C_S=30–40 Pa, while that of the flour was C_f=35 Pa. Angles of internal friction of the sand (ϕ_S=33°) and the flour (ϕ_f=43°) closely resemble those in natural rocks (ϕ=30–45°—Goodman, 1989). Time was not scaled in our experiments, as the brittle behaviour of sand and other Mohr–Coulomb materials is generally believed to be independent of strain rate.

2.3. Experimental procedures

A series of 'control' experiments was first conducted in the absence of regional stress to compare with experiments that incorporated regional extension or compression. The experimental procedure for collapse experiments free of regional stress began with inflation of the balloon via the air inlet pipe and its subsequent burial in the sandbox. The surface of the analogue material was then planed down until the balloon was located at the required depth, providing an even surface on which to observe fracture formation. The balloon was then deflated, by opening the valve on the air inlet pipe, to simulate reservoir evacuation and consequent subsidence of the overlying roof. Subsidence of 3–4 cm was almost

instantaneous, lasting 2–4 s in all experiments conducted. We regard this as equivalent to the subsidence rates inferred for major caldera forming eruptions in nature, in which down faulting of 1 or 2 km may occur over a period of days to hours (i.e., geologically instantaneous).

The experimental procedure for collapse experiments under regional stresses followed that of the control experiments up to burial of the inflated balloon and smoothing of the analogue material's surface. Compressive or extensional stresses were then applied to the sand medium by movement of the end walls until the desired amount of regional strain was achieved. Towards the end of the extension/compression phase, the balloon was deflated to simulate reservoir evacuation and accompanying caldera collapse. Balloon deflation was conducted syntectonically, with a half revolution of the driveshafts (equaling 2 mm displacement) over the course of caldera collapse so as to maintain regional stresses in the system. Measurements of model caldera dimensions were taken along axes orientated perpendicular to and parallel to the end walls, respectively termed the *A*-axis and *B*-axis (Fig. 3).

2.4. Limitations of the set-up

'Edge effects,' such as frictional forces operating around the surfaces of the deformation rig, can potentially disrupt scaling in analogue models. These effects were minimized in our experiments by the large size of the deformation rig (70–100 cm × 80 cm × 40 cm—Fig. 2), which permitted the studied deformation area (30 cm × 25 cm) in the center of the model to be sufficiently far away from the walls. The use of rubber balloons to simulate a magma chamber causes a separation of the chamber from its surroundings by an impenetrable membrane. This limits possible effects on collapse dynamics and pressure variations in a chamber due to subsidence of roof blocks. The crust immediately around the magma chamber is subjected to very high temperatures in nature, which could locally induce ductile behaviour. In our experiments, this section of the crust was assumed to behave in a brittle manner, the basis for which is that local strain rates involved in magma chamber inflation and deflation are typically

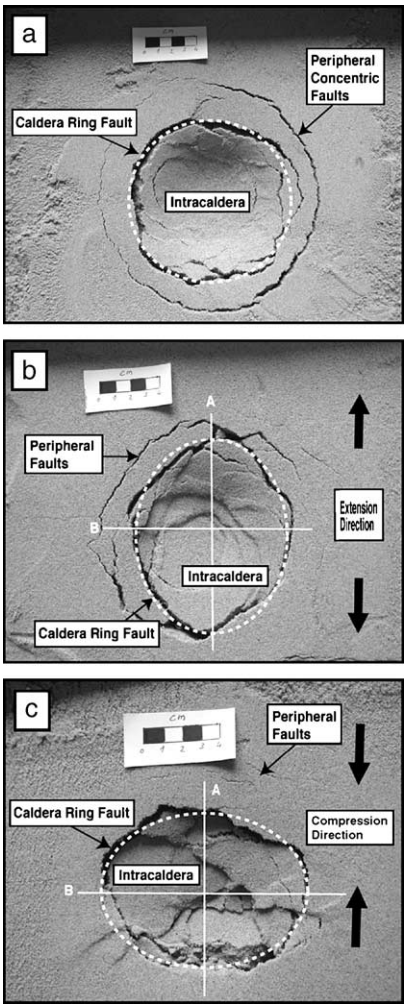

Fig. 3. Plan view photographs of model calderas made in sand under (a) stress-free conditions, (b) regional extension and (c) regional compression. The major axes of calderas in compression/extension experiments were denoted the *A*- and *B*-axes. The *A*-axis was taken as perpendicular to the end walls and the *B*-axis parallel to the end walls. Illumination is from the top of the photographs.

very high and would favour brittle deformation. A further assumption was that brittle behaviour in the crust extended regionally down to depths of 12 km or more. In nature, the brittle to ductile transition typically occurs between depths of 4 and 12 km. In areas of thickened crust, the transition may extend deeper than this range. Beneath the Southern Puna of the Central Volcanic Zone of the Andes for instance, the brittle–ductile transition is thought to be located at a depth of around 15 km (Seggiaro and Hongn,

1999). However, the transition is likely to be at the shallower end of this range in areas of high heat flow and thin crust. A follow-on to the assumption of brittle behaviour in the model is that time was assumed to exert little control in the style of deformation. In nature, however, rheology of crustal materials may deviate from Mohr–Coulomb behaviour and so our model cannot account for variation due to such effects. Strain in the model was assumed to be homogeneous, whereas concentrations of strain are likely in nature. Transtensional or transpressional tectonic regimes, with associated strike slip faulting, were not simulated using the above set-up and the impacts of pre-tectonic crustal anisotropies, doming due to magma chamber emplacement and pre-caldera topography (e.g., a conical volcanic edifice load) were not studied.

3. Experimental results

3.1. Caldera formation in a regional stress field

In the absence of far-field stress, calderas were predictably circular in plan (Fig. 3a). As in previous simulations cited above, caldera subsidence initially

Table 2
Results of experiments simulating caldera formation under regional compression and extension at 4 cm depth

Compression/extension experiments with balloon of radius 14 cm at 4 cm depth								Sand:Flour ratio=12:1			
Balloon depth [cm]	Driveshaft revs.	Strain [cm]	Strain [%]	Intracaldera (*I*)				Total morphological expression (*T*)			
				A-axis [cm]	*B*-axis [cm]	Aspect ratio (B/A)	Area of *I* [cm^2]	*A*-axis [cm]	*B*-axis [cm]	Aspect ratio	Area of *T* [cm^2]
No tectonics											
4	0	0.00	0.00	8.75	8.75	1.00	60.13	22.75	22.75	1.00	406.49
4	0	0.00	0.00	8.50	8.50	1.00	56.74	21.00	21.00	1.00	346.36
4	0	0.00	0.00	8.50	8.50	1.00	56.74	21.50	21.50	1.00	363.05
4	0	0.00	0.00	8.20	8.20	1.00	52.81	16.60	16.60	1.00	216.42
4	0	0.00	0.00	8.20	8.20	1.00	52.81	16.60	16.60	1.00	216.42
					Average	1.00	55.84		Average	1.00	309.75
Extension											
4	3	0.54	0.74	8.40	7.40	0.88	48.82	18.50	18.00	0.97	261.53
4	5	0.90	1.23	6.40	6.00	0.93	30.15	17.40	16.80	0.96	229.58
4	8	1.44	1.97	9.00	7.70	0.85	54.42	18.00	17.00	0.94	240.33
4	8	1.44	1.97	7.10	5.70	0.80	31.78	18.50	17.50	0.94	254.27
4	11	1.98	2.71	8.60	6.80	0.79	45.93	18.50	17.00	0.91	247.00
4	11	1.98	2.71	9.00	6.20	0.68	43.82	19.40	16.80	0.86	255.97
4	13	2.34	3.20	10.00	8.00	0.80	62.83	17.00	15.50	0.91	206.95
4	13	2.34	3.20	9.8	7	0.71	53.87	15	13.50	0.90	159.04
4	15	2.70	3.69	6.60	6.00	0.90	31.10	19.50	17.70	0.90	271.08
4	17	3.06	4.19	9.00	6.50	0.72	45.94	17.50	15.00	0.85	206.16
					Average	0.81	44.87		Average	0.91	233.19
Compression											
4	3	0.54	0.74	7.10	7.50	1.05	41.82	15.50	16.50	1.06	200.86
4	5	0.90	1.23	7.5	8	1.06	47.12	17.4	17.8	1.02	243.25
4	8	1.44	1.97	5.5	6.6	1.20	28.51	15.5	16.5	1.06	200.86
4	11	1.98	2.71	7	7.5	1.07	41.23	16.5	18.7	1.13	242.33
4	13	2.34	3.20	6.5	7	1.07	35.73	17.9	18.5	1.03	260.08
4	15	2.70	3.69	5.70	7.00	1.22	31.33	16.00	17.80	1.11	223.68
4	17	3.06	4.19	7.20	8.40	1.16	47.50	17.00	18.00	1.05	240.33
4	19	3.42	4.68	5.4	7.40	1.37	31.38	15.70	17.5	1.11	215.78
					Average	1.15	38.08		Average	1.07	228.40

occurred as a central zone of downsag accompanied by an outer concentric zone of tensional fractures. Downsag subsequently progressed into collapse along outward-dipping reverse faults in the intracaldera, accompanied by normal faulting in the peripheral zone.

In experiments simulating extensional tectonic regimes, an evenly spaced series of fractures formed across the analogue medium, orientated parallel to the moving end walls. At higher regional strain levels, these fractures developed into normal faults that defined a horst and graben pattern. In compressive regimes, a similarly equally spaced series of reverse fractures (albeit fewer in number) formed parallel to the end walls. Calderas produced from circular magma chambers in both the compression and extension experiments were elliptical in shape and typically elongate parallel to the direction of least horizontal compressive stress—hereafter denoted ShMin (Fig. 3b and c). For experiments with regional extension, ShMin is parallel to the regional extension direction, while for experiments with regional compression, ShMin is perpendicular to the regional compression direction.

Data sets representative of the experimental series are given in Tables 2 and 3. The tables show that the average intracaldera area formed under extension and compression increases with decreasing depth. This can be related to the level at which the outward dipping (bell-shaped) reverse ring fault(s) that bound the intracaldera intersect the sand surface (cf. Walter and Troll, 2001). In contrast, the average area of the normal fault bound peripheral zone decreases with decreasing depth. Another feature of the data is that the average area encompassed by intracalderas formed in compression is slightly lower relative to those

Table 3
Results of experiments simulating caldera formation under regional compression and extension at 2.5 cm depth

Compression/extension experiments with balloon of radius 14 cm at 2.5 cm depth								Sand:Flour ratio=12:1			
Balloon depth [cm]	Revolutions	Strain [cm]	Strain [%]	Intracaldera (*I*)				Total morphological expression (*T*)			
				A-axis [cm]	*B*-axis [cm]	Aspect ratio (B/A)	Area of *I* [cm^2]	*A*-axis [cm]	*B*-axis [cm]	Aspect ratio (B/A)	Area of *T* [cm^2]
No tectonics											
2.5	0	0.00	0.00	7.30	7.20	0.98	41.28	18.00	18.00	1.00	254.46
2.5	0	0.00	0.00	7.20	7.30	1.01	41.28	18.00	18.00	1.00	254.46
					Average	1.00	41.28		Average	1.00	254.46
Extension											
2.5	3	0.54	0.74	8.30	7.40	0.89	48.23	17.00	16.50	0.97	220.30
2.5	5	0.90	1.23	7.50	7.00	0.93	41.23	16.80	16.00	0.95	211.11
2.5	8	1.44	1.97	8.20	6.10	0.74	39.28	17.80	16.50	0.92	230.67
2.5	11	1.98	2.71	7.60	6.50	0.85	38.79	17.70	16.20	0.91	225.20
2.5	13	2.34	3.20	9.5	8.7	0.91	64.91	18.5	17.00	0.91	247.00
2.5	15	2.70	3.69	8.00	6.70	0.83	42.09	17.50	15.20	0.86	208.91
2.5	17	3.06	4.19	8.75	7.25	0.82	49.82	16.50	14.00	0.84	181.42
					Average	0.85	46.34		Average	0.91	217.80
Compression											
2.5	3	0.54	0.74	6.80	7.10	1.04	37.91	16.50	17.40	1.05	225.48
2.5	5	0.90	1.23	7.70	7.90	1.02	47.77	17.40	18.40	1.05	251.45
2.5	8	1.44	1.97	6.50	6.80	1.04	34.71	16.25	17.25	1.06	220.15
2.5	11	1.98	2.71	5.90	6.75	1.14	31.27	16.20	17.50	1.08	222.66
2.5	13	2.34	3.20	5.50	7.20	1.30	31.10	16.70	17.75	1.06	232.81
2.5	15	2.70	3.69	7.40	8.50	1.14	49.40	16.50	17.80	1.07	230.67
2.5	17	3.06	4.19	7.20	8.50	1.18	48.06	16.50	18.50	1.12	239.74
2.5	19	3.42	4.68	7.75	10.50	1.35	63.91	15.50	17.25	1.11	209.99
					Average	1.15	43.02		Average	1.07	229.12

formed in extension. This may well be due to a slight thickening of the sand pile during the pre-collapse regional compression phase. A corresponding increase in the average peripheral areas in compression relative to those in extension is also shown in Table 3, while its absence in Table 2 may simply be a function of variability in that particular dataset.

Thus the area of calderas formed in stressed and non-stressed experiments was controlled by depth and initial plan view area of the underlying magma chamber (Fig. 4a). The areas encompassed by the intracaldera and the peripheral fault zones in stressed experiments remained approximately constant with (and therefore independent of) increasing pre-collapse regional strain (Fig. 4b). However, calderas formed in experiments with regional stress appeared increasingly elliptical in plan with increasing pre-collapse regional strain. A positive linear relationship between the total regional strain and ellipticity of the model calderas was observed (Fig. 4c). The ellipticity of the intracaldera tended to be more pronounced than that of the corresponding peripheral zone for a given value of regional strain. This discrepancy became larger with increasing regional strain.

3.2. Interaction of caldera-related and regional fault patterns

A significant influence on the development of caldera structures encountered during some experiments was the presence of pre-existing regional faults. In experiments simulating extensional tectonic regimes, several key observations were made where normal faults bounding horsts and grabens intersected the area affected by the developing caldera. Firstly, pre-existing normal faults intersecting the edge of the developing caldera were frequently re-used (sometimes with motion reversed) to accommodate the subsidence of the collapsing chamber roof. This was especially the case in experiments with lower sand/flour ratios where such normal faults dipped in the preferred orientation of reverse ring faults (Fig. 5). Where such regional faults became caldera-bounding faults, significant truncation or distortion of the preferred elliptical–subcircular surface expression was observed, with displacement along ring fractures taken up by regional faults instead. Secondly, concentric extensional fractures in the caldera periphery

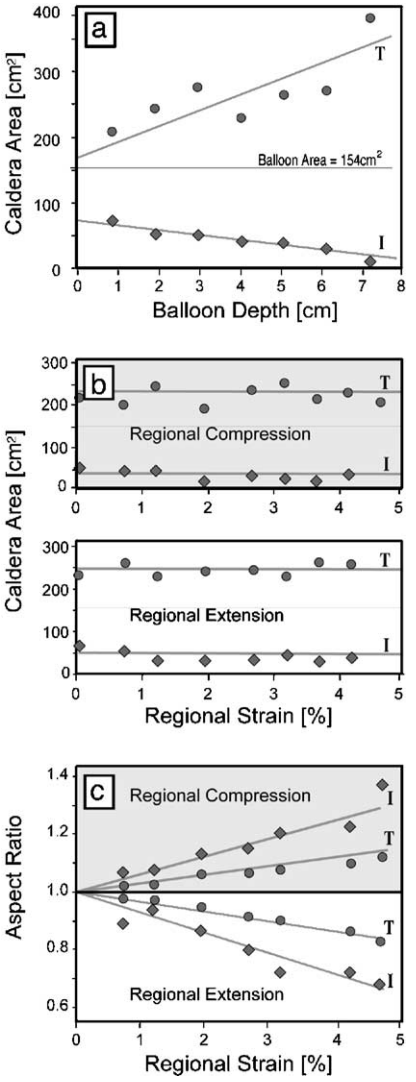

Fig. 4. (a) Plot of change in caldera areas with reservoir burial depth. The area of the intracaldera (*I*) decreases with depth (as it is bound by reverse faults), whereas the overall morphological expression (*T*) increases with depth. (b) Plots showing model caldera areas are independent of regional strain. Regional strain (e_R) perpendicular to the end walls was measured as a percentage, given by the initial length (l_o) of the sand-box subtracted from the final length (l_f) and then divided by the initial length [i.e., $e_R=(l_f-l_o)/l_o$]. (c) Plot showing a change in aspect ratios (*B*-axis/*A*-axis) of intracaldera (*I*) and total morphological expressions (*T*) of the calderas with increasing regional strain. {Data in panels (b) and (c) from experiments run with a magma chamber of 14 cm in diameter (plan view area, A=155 cm^2) at depth of 4 cm in a 12:1 sand/flour mix—see Table 2}.

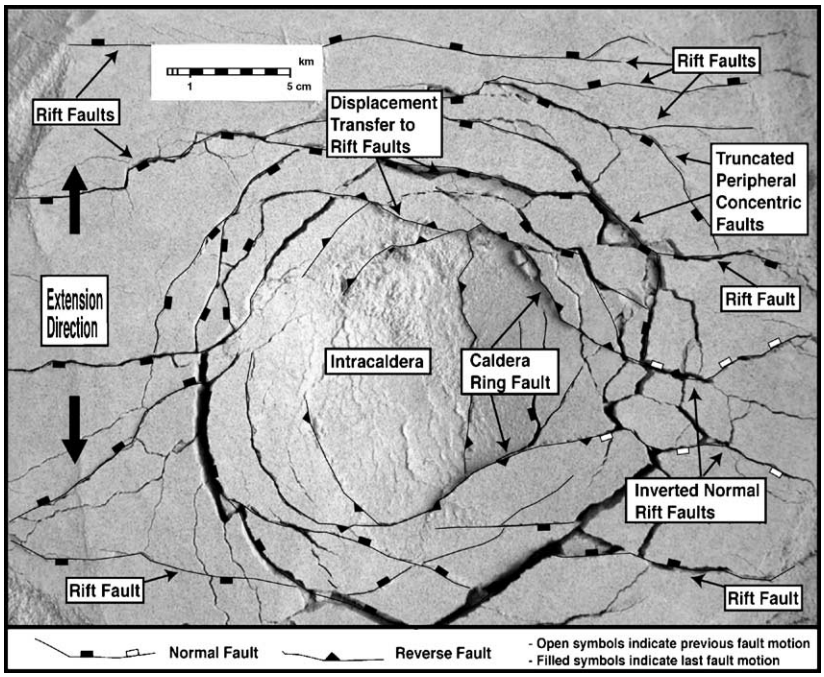

Fig. 5. Plan view photograph showing interaction of pre-existing regional structures with caldera structures, resulting from caldera collapse under regional extension in a medium composed of a 3:1 sand/flour ratio. Illumination is from the right of the photograph. Note the truncation of peripheral and intracaldera faults by the regional structures. Note also the eastward projection of the caldera depression via the formation of a graben along inverted regional normal faults.

were consistently 'captured' or re-orientated during their propagation in the proximity of pre-existing normal faults. The regional normal faults also accommodated some peripheral extension during collapse of the intracaldera, particularly at the ends of the caldera's *A*-axis. Thirdly, the floor of the caldera sometimes subsided as discrete blocks ("piecemeal subsidence") rather than as a coherent block, due to the existence of pervasive regional fractures prior to collapse. The locally compressive stress regime in the subsiding intracaldera basin resulted in differential down faulting of these blocks (some appearing as fault-bound 'pop-ups' within the caldera floor), forming irregular and stepped caldera floor topographies.

Continued regional extension or compression after collapse led to progressive distortion of the newly formed caldera structure, causing it to be even further elongated. This process affected the caldera area however, progressively increasing the *A*-axis length in extensional experiments and decreasing the *A*-axis length in compressive experiments.

4. Discussion

Analogue experiments were conducted to examine one of the possible mechanisms for the formation of elongate calderas under regional stress—'fault distortion'. In the absence of regional forces, the local stress field due to a deflating (or inflating) oblate or spherical magma chamber will produce a circular caldera, consistent with earlier theoretical studies (e.g., Gudmundsson et al., 1997) and physical modelling experiments (e.g., Roche et al., 2000; Acocella et al., 2000; Walter and Troll, 2001). Our experiments investigated the effects of regional stresses and associated structures on the local fault pattern produced during evacuation collapse of a magma chamber of known dimensions. The key observation of our pure collapse experiments was that elliptical calderas formed above circular magma chambers when subjected to regional stress during formation. This suggests a distortion of the local stress field associated with the collapsing balloon due to interaction with a far-field stress regional regime.

4.1. Influence of far-field stress on local caldera structures—'fault distortion' and possible implications

Two or more stress fields can interact to produce a combined or composite stress field (Park, 1997). Analogue studies conducted by van Wyk de Vries and Merle (1996, 1998) examined the effects of volcanic loads on regional fault patterns associated with orthogonal and pull-apart (strike slip) rifting. These studies show interplay between the local volcanic and regional stress regimes, the result of which is the distortion of regional and local fault trajectories in the vicinity of the superimposed stress fields. We propose that a similar distortion effect may account for the structures produced in our simulations of caldera collapse under regional stress.

For our experiments, the stress fields to consider are (1) a local stress field associated with the deflating magma chamber and (2) a regional stress field, due to either regional extension or far-field shortening. A qualitative two-dimensional mechanical analysis of the observed reverse ring fault patterns along the *A*- and *B*-axes of the experimental set-up is schematically presented in Fig. 6. This analysis is based on the experiments with regional extension only, but, as the results from regional compression experiments essentially mirror those of the regional extension experiments, the analysis can be reversed to account for ring fault patterns produced in regional compression. Following the convention of van Wyk de Vries and Merle (1996, 1998), we define the principal axes of stresses induced by the collapsing chamber σ_V, those for regional stresses are symbolised by σ_R and the combined stresses are represented by σ_C.

The deflation of the balloon is characterized by a greater rate of contraction over its center with respect to its margins (Fig. 6a). This disparity results in shearing of the down-going roof, and creation of a main local compressive stress, $\sigma 1_V$, at 45° to the applied shear. According to the Coulomb criterion, shear fractures will develop at an angle of 30–35° to $\sigma 1_V$, and thus dip steeply outward (~75°) with a reverse motion (cf. Roche et al., 2000).

The stress field resulting from orthogonal regional extension is characterized by a vertical main compressive stress, $\sigma 1_R$, and a horizontal least compressive stress, $\sigma 3_R$ (Fig. 6b). Interaction of the regional and local stress fields produces resultant (combined) principal stress axes, $\sigma 1_C$ and $\sigma 3_C$, which are rotated outward relative to $\sigma 1_V$ and $\sigma 3_V$. The degree of rotation will depend on the relative magnitudes of the local and regional stresses. As a consequence, the reverse fault orientation is also rotated outward and its dip steepened. If the caldera-bounding reverse fault is steeper, it will intersect the surface at a greater distance from the caldera center, resulting in an elongation of the caldera radius in the *A*-direction (Fig. 3a).

The extension of the deformation rig causes the rubber base to contract in the *B*-direction. This contraction exerts a regional stress on the sand defined by a horizontal main compressive stress, $\sigma 2_R$, and vertical least compressive stress, $\sigma 3_R$. Therefore, the opposite occurs to what happens along the *A*-axis, with $\sigma 1_C$ and $\sigma 3_C$ rotated inward along the *B*-axis relative to $\sigma 1_V$ and $\sigma 3_V$. This results in a shallowing of the ring fault, which, when the fault reaches the surface, causes shortening of the caldera radius in the *B*-direction. For chamber collapse under regional compression, the situation along the *A*- and *B*-axes is reversed and so the caldera is elongated along the *A*-axis and shortened along the *B*-axis (Fig. 6c).

The discrepancy between the ellipticities of the intracaldera area and the surrounding peripheral fault zone (Fig. 4b) is related to the horizontal displacement or heave along the reverse ring faults. The steeper the reverse ring fault, the less its heave and, correspondingly, the less extension is exerted in its periphery. For the case of regional extension, reverse ring faults are steepest at the ends of the *A*-axis. As this is where the horizontal displacement along the ring fault is least, the outward extent of the peripheral fault zone will be shortest. The opposite occurs along the *B*-axis, where the heave on the ring fault is greatest and so the outward extent of the peripheral fault zone will be greatest. The result is a peripheral fault zone that has an aspect ratio less than that of the intracaldera it encloses. With increasing regional strain, the disparity in aspect ratios increases (Fig. 4b). This can be related to a consequent increased steepening of the reverse fault sections facing the ShMin and the increased shallowing of those sections facing the main regional horizontal compressive stress (ShMax).

The circumferential variation in ring fault dip due to 'fault distortion' – or perhaps more accurately,

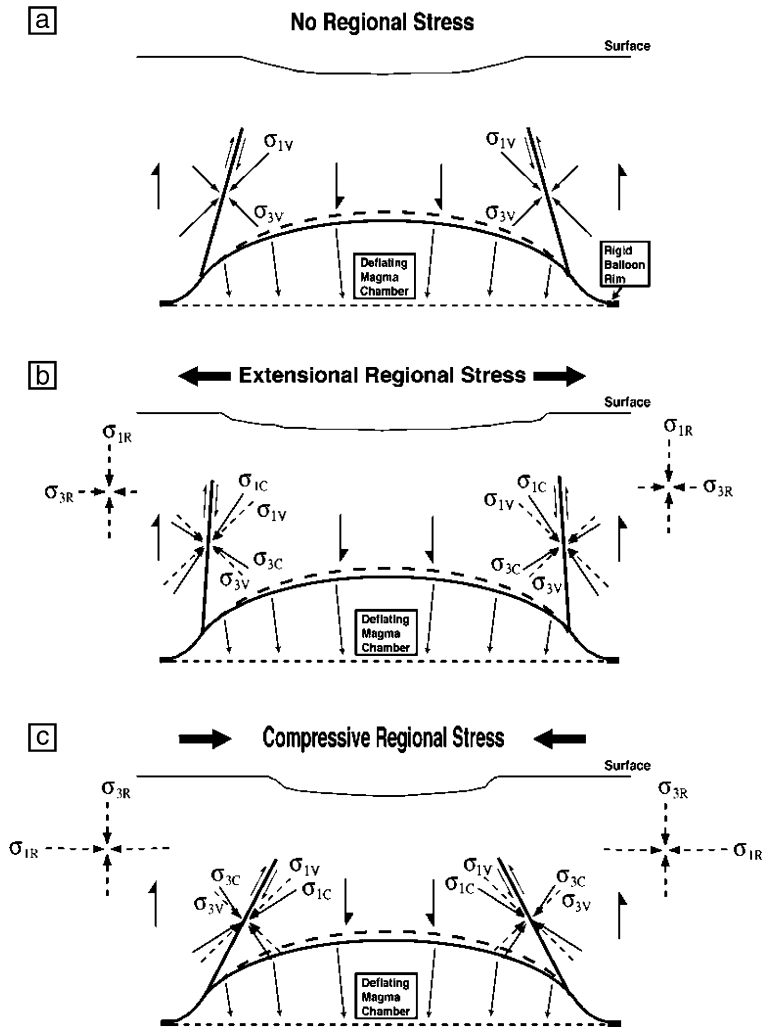

Fig. 6. A 2D analysis of the 'fault distortion': (a) chamber deflation without tectonic stress. The black arrows in the chamber schematically represent contraction velocities. Faster deflation of the balloon over its center sets up two shear zones at the margins of the down-going roof. Outward-dipping reverse ring fractures (Riedel shears) propagate at ~30° to the main local compressive stress $\sigma 1_V$ to accommodate collapse (cf. Roche et al., 2000). (b) Chamber deflation under extensional tectonic stress in section view parallel to the regional extension direction. Superposition of a regional stress with a vertical main compressive stress axis, $\sigma 1_R$ results in a composite main compressive stress axis $\sigma 1_C$, which has been rotated outward relative to the main local compressive stress axis $\sigma 1_V$. The steeper $\sigma 1_C$ produces steeper reverse faults, which elongate the caldera structure in the direction of regional extension. (c) Chamber deflation under compressive tectonic stress in section view parallel to the regional compression direction. Superposition of a vertical main regional compressive stress axis, $\sigma 1_R$ on the local stress field results a composite main compressive stress axis $\sigma 1_C$, which has been rotated inward relative to the main local compressive stress axis $\sigma 1_V$. The shallower $\sigma 1_C$ produces correspondingly shallower reverse faults, which shorten the caldera structure in the direction of regional compression.

'local stress field distortion' – may have significant implications for syn- and post-caldera ring fault eruptions. Magma may be injected along fractures if the magma pressure exceeds the compressive stress across the fracture plane (Park, 1997). During vertical subsidence of the intracaldera zone, the tensional component across a subsidence-controlling reverse ring fault will be greatest where the reverse fault dips most shallowly. Our experiments suggest that reverse ring faults will be shallowest where they

strike perpendicular to the ShMax. It seems likely therefore that injection of magma along an elliptical reverse ring fault, forming due to caldera collapse under regional stress, will preferentially occur along the fault sections facing the regional ShMax.

Once formed, natural calderas remain subject to the regional forces that acted during collapse. Our experiments showed that continuing regional strain increases the ellipticity of the newly formed caldera structure by further elongating it. Therefore, post-caldera regional deformation is likely to add to the 'distortion' of caldera structures. This effect in altering the ellipticity of a caldera is likely to be more pronounced with increasing age of the caldera structure, increased duration of regional strain and increasing regional strain rate.

Finding field evidence for the occurrence of such a 'fault distortion' effect at calderas in nature is likely to be difficult. Mapping the ring faults at calderas to see if dips change as predicted in our model is commonly hindered by limited exposure. Alternatively, comparison of a caldera's structural dimensions with the dimensions of the magma chamber that lies beneath would be required. It may be possible to image the chamber remnants beneath a caldera using geophysical techniques and compare its geometry with that of the caldera. However, a major uncertainty of this approach is whether the original chamber into which collapse occurred is being imaged and has not been already modified or even destroyed during or after caldera formation (cf. Wolff and Gardner, 1995).

While the fault distortion effect is likely to apply to reservoirs of any geometry, we believe the initial magma chamber dimensions will still exert a fundamental control on caldera geometry. Assuming Newtonian behaviour, a viscous material like magma will deform under the slightest differential stress (Twiss and Moores, 1992), while even a more realistic non-Newtonian fluid character will also permit flow and deformation, once yield strength is exceeded. Newhall and Dzurisin (1988) quote natural examples of caldera floor uplift and subsidence that have been related to 'squeezing' or stretching of magma chambers resulting from regional strain. It is therefore conceivable that magma chambers that are non-circular in plan view underlie natural calderas in tectonically active regions. One aspect of future work must be to more fully understand what controls initial geometry of a magma chamber in tectonically active settings.

4.2. Role of pre-existing structures

In our experiments, the reactivation of pre-existing regional structures also played a role in the formation of model calderas. In general, their influence related to the frequent development of three features of the model calderas: (1) the formation of a segmented, 'piecemeal' caldera floor with variable down faulting of neighbouring blocks, (2) the truncation of caldera ring faults and (3) the creation of a distinctly polygonal caldera outline. Ramberg's (1981) centrifuge experiments demonstrated the capacity for pre-existing fractures to accommodate caldera-like subsidence without the generation of new fractures. The development of many natural calderas is clearly influenced by faults parallel to regional trends (see Section 4.3 below).

Where piecemeal caldera collapse was observed (Fig. 3c), individual blocks in the caldera floor were bounded by a combination of local caldera faults and pre-existing regional fractures. This type of piecemeal caldera subsidence differs from the more regular pattern observed in experiments simulating cyclic doming and collapse (Walter and Troll, 2001; Troll et al., 2002), where radial segmentation of the caldera floor occurs due to faulting resulting from phases of doming. In some of our experiments, truncation of caldera ring faults occurred when regional faults accommodated collapse, preventing the generation of a complete ring fracture. In these experiments, displacement transfer from ring fractures to regional structures was also observed (Fig. 5), where a complete ring fracture was initially generated, but the major displacement was nonetheless accommodated along the regional faults. A similar reactivation and utilisation of regional faults by caldera ring faults was observed in analogue experiments that simulated caldera formation and resurgence in sand deformed by pre-existing extensional faults (Acocella et al., 2004). In these experiments, such reactivation contributed to the elongation of a caldera's surface expression.

A subordinate feature observed in experiments was the 'capture' or propagation of some (particularly peripheral) caldera faults toward pre-existing regional

faults, which can perhaps be explained in terms of the tendency of fractures to propagate toward free surfaces or discontinuities. Alternatively, this phenomenon could be related to the switchover from a composite stress regime dominated by the deflating magma chamber to one where the regional stresses again become more dominant.

Based on his experiments, Komuro (1987) discussed the formation of polygonal calderas purely due to doming. In his model, perpendicularly intersecting radial and concentric faults, generated by the near-field stresses of magma chamber inflation, result in the formation of a polygonal caldera at the apex of the domed region. For caldera formation only due to magma chamber deflation, however, the formation of radial faults is unlikely to occur (Walter and Troll, 2001). In addition, although the formation of some natural calderas has indeed been associated with tumescence (Troll et al., 2000), others apparently show little evidence of pre-collapse doming (Lipman, 1984). Hence, theoretically at least, polygonal outlines of natural calderas that lack evidence for major pre-collapse uplift may more likely be controlled by intersection of regional and caldera faults, such as seen in our experiments.

4.3. Comparison of experimental results with natural examples

Calderas that are elongate parallel or sub-parallel to the regional minimum horizontal compressive stress can be found in extensional as well as in compressive settings. Examples of such calderas in extensional settings include Valles caldera, New Mexico (Goff and Gardner, 1994; Aldrich et al., 1986), Furnas caldera, Sao Miguel Island Azores (Guest et al., 1999), Suswa caldera, Kenyan Rift Valley (Skilling, 1993; Bosworth et al., 2000), and Taupo caldera, New Zealand (Wilson et al., 1995). Of these examples, the Taupo caldera most closely matches the calderas and extensional tectonic regime produced in our experiments (Fig. 7a). Field and remote sensing data gathered by Acocella et al. (2003) show that Taupo caldera lies in a segment of the Taupo Volcanic Zone rift, along which extension is purely orthogonal to the rift axis (i.e., no strike slip component—as in our experiments).

Examples of calderas located in compressive regimes appear to be far less common. One example is the Katmai caldera, Alaska (Fig. 7b). Katmai is also elongate parallel to the regional minimum horizontal compressive stress (Wallmann et al., 1990). Caldera collapse at Katmai occurred due to lateral withdrawal of magma from beneath the volcano and its distal eruption through the Novarupta vent in 1912 (Hildreth and Fierstein, 2000). The structural data (joint and dyke orientations) collected by Wallmann et al. (1990) imply that the compression direction around Katmai is more or less orthogonal to the volcanic axis of the Aleutian Arc. Thus, the eruption scenario at Katmai and the resultant caldera surface expression are quite similar to that simulated in our experiments. It is also notable that the surface expression of the Novarupta vent (a collapse feature) is also elliptical and elongate in the same orientation as Katmai caldera, as would be predicted from the above experimental results.

Many calderas are not located in areas of orthogonal or pure extension as is the case in our model. Some, for instance Gariboldi and Gedemsa calderas in the Ethiopian rift (Acocella et al., 2002), lie in regions undergoing extension oblique to the rift axis and are themselves elongated at an oblique angle to the rift and the extension direction. The caldera orientations in this scenario may be explained by magma chamber elongation along deep-rooted strike slip faults accommodating the oblique extension direction. Others, like Kapenga caldera, New Zealand (Acocella et al., 2003), are clearly elongated parallel to the major extensional/strike slip faults of the rift axis and are subperpendicular to the regional extension direction. This implies pre-existing fault orientation as the major control on magma chamber and/or caldera elongation for such examples. Conversely, the massive Cerro Galan caldera, NW Argentina (Francis et al., 1978; Marrett et al., 1994—Fig. 7c), which formed under an initially transpressive tectonic regime, is elongate parallel to regional fault and crustal lineament trends, but also parallel to the regional ShMin at the time of its formation. The tectonic history of the region around Cerro Galan has been quite complex and perhaps serves as a note of caution that one must carefully distinguish between current stress regimes and those at the time of caldera formation.

Some calderas in transtensional tectonic settings, while not elongate parallel to the regional minimum compressive stress, may be elongated parallel to a more localised minimum compressive stress resulting from second order tectonic movements. An example is the Somma–Vesuvius caldera complex, where the earliest collapse structure has a long axis trending obliquely (ESE–WNW) to the regional minimum compressive stress (NNE–SSW) of the surrounding Campanian Plain (Bianco et al., 1998; Cioni et al., 1999). In this case, regional extension is accommodated by two sets of perpendicularly intersecting oblique-normal faults. Sense of shear on these fault trends is opposite (conjugate), which generates a zone of localised ESE–WNW extension around the Somma–Vesuvius complex.

The influence of pre-existing regional fault patterns on caldera surface expression can be seen in many natural calderas. Regional faults may impact on the geometry of a caldera by defining the boundaries of the underlying magma chamber, which may then exert the main control on caldera geometry (see above) or by providing lines of weakness that can be exploited by a forming ring fault. For example, the first major collapse at the Campi Flegrei Caldera, Italy, was accommodated to a very significant degree along pre-existing, regional oblique-slip normal faults (Orsi et al., 1996), as was the 1883 collapse at Krakatau, Indonesia (Deplus et al., 1995). Regional

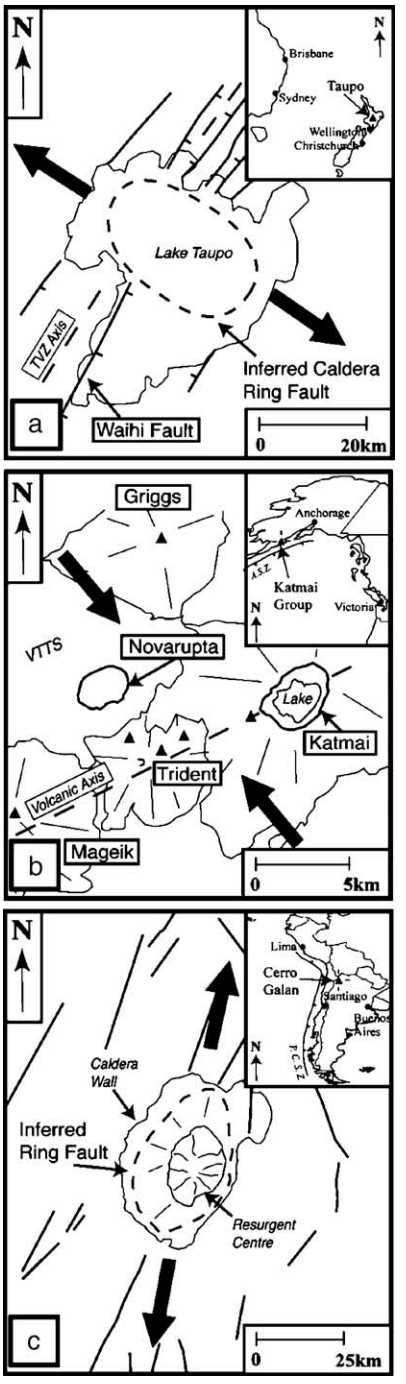

Fig. 7. (a) Sketch map of Taupo caldera, New Zealand (redrawn from Cole et al., 1998; Acocella et al., 2003). Taupo, like the calderas produced in our experiments, was formed under orthogonal extension and is elongated parallel to the regional least compressive stress. The volcano-tectonic half-graben, which extends southwest from the caldera and is bounded by the pre-existing regional Waihi fault, closely resembles a similar feature observed in some of our model calderas (Fig. 5). TVZ—Taupo volcanic zone. (b) Sketch map of the Katmai Volcanic Cluster (redrawn from Hildreth and Fierstein, 2000; Wallmann et al., 1990). Situated in an area of orthogonal compression, the Katmai caldera and the collapsed area around the associated Novarupta vent are both elongate perpendicular to the regional main compressive stress, as was the case for model calderas in our experiments. Black triangles are peaks ASZ—Aleutian Subduction Zone. (c) Sketch map of Cerro Galan caldera, NW Argentina. Cerro Galan was most likely located in an area of transpressional tectonics at the time of its initial formation. Like Katmai caldera and in our experiments, it is elongated parallel to the least compressive stress. Cerro Galan is also orientated parallel to the major crustal lineaments in the area, however suggesting that these could have played role in controlling its subsidence geometry. Magma chamber elongation either along basement faults or through the borehole break out mechanism could also be responsible for this particular caldera's surface geometry. PCSZ—Peru–Chile Subduction Zone.

extensional/strike slip faults are also regarded as the primary control on the subsidence of the massive Toba caldera, Indonesia (Aldiss and Ghazali, 1984), and hence its direction of elongation.

A variation on this theme is seen in Fig. 5, where the main ring fault is observed to splay out eastward to join up with two regional normal faults, resulting in the down faulting of a radial graben extending into the periphery. The Taupo caldera, New Zealand, is characterized by a similar down-faulted half-graben extending southeast from the area bound by the main ring fault (Cole et al., 1998—Fig. 7a). Campi Flegrei caldera also exhibits this splaying-out of caldera faults toward regional faults with resultant volcano-tectonic graben subsidence in the periphery. True ring faults play a role in all of the above examples, but the extent to which they accommodate subsidence in calderas under regional stress is very variable.

A further product of the intersection of regional faults with the caldera structures in the experiments is the dissection of the caldera floor by regional faults. This often resulted in a random piecemeal caldera floor structure, a feature very similar to that observed by Branney and Kokelaar (1994) at Scafell caldera in the English Lake District and by Moore and Kokelaar (1998) at Glencoe caldera, Scotland. The influence of regional structures can also be seen on doming, for example, in the polygonal morphology of the dome on the island of Ischia, Italy, which is strongly controlled by intersecting regional faults (Acocella and Funiciello, 1999). These combined experimental and field observations thus underline the importance of pre-existing and syn-tectonic regional structures in volcano-tectonic processes.

5. Conclusions

From the experimental observations above, we imply that distortion of caldera ring faults may be of great significance for caldera formation in active tectonic regimes. This distortion may occur in three main ways:

1) Elongation of the concentric caldera ring and peripheral fault systems in the direction of least horizontal compressive stress (ShMin).
2) Truncation and ‘capture’ of ring and peripheral faults by the pre-existing fault systems associated with the regional stress field.
3) Post-collapse deformation of the caldera structures due to regional strain.

As a consequence of the stress-related distortion, ring fault orientation varies from steeply dipping when facing the ShMin, to shallower dips when facing the ShMax. This variation of caldera fault dip may play a role in the localization of eruptions or intrusions along such an elliptical ring fissure.

Distinction between the precise roles played by caldera fault distortion and elliptical magma chamber growth at a particular caldera in nature may be difficult. This is due to the potentially complementary effects of these mechanisms on the caldera structure produced. Only detailed analysis of further field and experimental data will resolve the relative importance of either mechanism in nature.

Acknowledgements

We would like to thank Aisling Soden and Jonathan Moore for their assistance in the laboratory, and John Graham for his support and advice. Discussion with John Wolff and Valerio Acocella was both very helpful and greatly appreciated. We also thank Agust Gudmundsson, Franck Donnadieu and William Bosworth, whose thorough reviews greatly enhanced the paper. Grants from Trinity College to VRT and EPH, and project support from the German Science Foundation to TRW (DFG grant WA1642) are gratefully acknowledged. EPH also acknowledges support from the Irish Geological Association and from the Volcanic and Magmatic Studies Group, UK.

References

Acocella, V., Funiciello, R., 1999. The interaction between regional and local tectonics during resurgent doming; the case of the island of Ischia, Italy. Journal of Volcanology and Geothermal Research 88, 109–123.

Acocella, V., Cifelli, F., Funiciello, R., 2000. Analogue models of collapse calderas and resurgent domes. Journal of Volcanology and Geothermal Research 104, 81–96.

Acocella, V., Korme, T., Salvini, F., Funiciello, R., 2002. Elliptic calderas in the Ethiopian rift: control of pre-existing structures. Journal of Volcanology and Geothermal Research 119, 189–203.

Acocella, V., Spinks, K., Cole, J.W., Nicol, A., 2003. Oblique back arc rifting of Taupo Volcanic Zone, New Zealand. Tectonics 22, 1045.

Acocella, V., Funiciello, R., Marotta, E., Orsi, G., de Vita, S., 2004. The role of extensional structures on experimental calderas and resurgence. Journal of Volcanology and Geothermal Research 129, 199–217.

Aldiss, D.T., Ghazali, S.A., 1984. The regional geology and evolution of the Toba volcano-tectonic depression, Indonesia. Journal of the Geological Society (London) 141, 487–500.

Aldrich, M.J., Chapin, C.E., Laughlin, A.W., 1986. Stress history and tectonic development of the Rio Grande Rift, New Mexico. Journal of Geophysical Research 91B, 6199–6211.

Anderson, E.M., 1936. The dynamics of the formation of cone sheets, ring dikes, and cauldron subsidences. Proceedings of the Royal Society of Edinburgh 56, 128–163.

Belousov, A., Walter, T.R., Troll, V.R., 2004. Large scale failures on domes and stratocones situated on caldera ring faults: sandbox modeling of natural examples from Kamchatka, Russia. Bulletin of Volcanology (online).

Bianco, F., Castellano, M., Milano, G., Ventura, G., Vilardo, G., 1998. The Somma–Vesuvius stress field induced by regional tectonics: evidences from seismological and mesostructural data. Journal of Volcanology and Geothermal Research 82, 199–218.

Bosworth, W., Burke, K., Strecker, M., 2000. Magma chamber elongation as an indicator of intraplate stress field orientation: "borehole break-out mechanism" and examples from the Late Pleistocene to Recent Kenya Rift Valley. Journal of the Virtual Explorer 2 (Online-http://virtualexplorer.com.au).

Bosworth, W., Burke, K., Strecker, M., 2003. Effect of stress fields on magma chamber stability and the formation of collapse calderas. Tectonics 22, 1042.

Branney, M.J., 1995. Downsag and extension at calderas: new perspectives on collapse geometries from ice-melt, mining, and volcanic subsidence. Bulletin of Volcanology 57, 303–318.

Branney, M.J., Kokelaar, P., 1994. Volcanotectonic faulting, soft-state deformation, and rheomorphism of tuffs during development of a piecemeal caldera, English Lake District. Geological Society of America Bulletin 106, 507–530.

Cailleau, B., Walter, T.R., Janle, P., Hauber, E., 2003. Modeling volcanic deformation in a regional stress field: implications for the formation of graben structures on Alba Patera, Mars. Journal of Geophysical Research 108, 5141.

Cioni, R., Santacroce, R., Sbrana, A., 1999. Pyroclastic deposits as a guide for reconstruction of the multi-stage evolution of the Somma–Vesuvius Caldera. Bulletin of Volcanology 61, 207–222.

Cole, J.W., Brown, S.J.A., Burt, R.M., Beresford, S.W., Wilson, C.J.N., 1998. Lithic types in ignimbrites as a guide to the evolution of a caldera complex, Taupo volcanic centre, New Zealand. Journal of Volcanology and Geothermal Research 80, 217–237.

Deplus, C., Bonvalot, S., Dahrin, D., Diament, M., Harjono, H., Dubois, J., 1995. Inner structure of the Krakatau volcanic complex (Indonesia) from gravity and bathymetry data. Journal of Volcanology and Geothermal Research 64, 23–52.

Francis, P.W., Hammill, M., Kretzschmar, G., Thorpe, R., 1978. The Cerro Galan Caldera. North-west Argentina and its tectonic setting. Nature 274, 749–751.

Goff, F., Gardner, J.N., 1994. Evolution of a mineralized geothermal system, Valles Caldera, New Mexico. Economic Geology and the Bulletin of the Society of Economic Geologists 89, 1803–1832.

Goodman, R.E., 1989. Introduction to rock mechanics, 2nd ed. John Wiley and Sons, New York. 562 pp.

Gudmundsson, A., 1988. Formation of collapse calderas. Geology 16, 808–810.

Gudmundsson, A., 1998. Formation and development of normal-fault calderas and the initiation of large explosive eruptions. Bulletin of Volcanology 60, 160–170.

Gudmundsson, A., Marti, J., Turon, E., 1997. Stress fields generating ring faults in volcanoes. Geophysical Research Letters 24, 1559–1562.

Guest, J.E., Gaspar, J.L., Cole, P.D., Queiroz, G., Duncan, A.M., Wallenstein, N., Ferreira, T., Pacheco, J.M., 1999. Volcanic geology of Furnas Volcano, São Miguel, Azores. Journal of Volcanology and Geothermal Research 92, 1–29.

Hildreth, W., Fierstein, J., 2000. Katmai volcanic cluster and the great eruption 1912. Geological Society of America Bulletin 112, 1594–1620.

Hubbert, M.K., 1951. Mechanical basis for certain familiar geologic structures. Geological Society of America Bulletin 62, 355–372.

Kennedy, B., Stix, J., Vallance, J.W., Lavallée, Y., Longpré, M.-A., 2004. Controls on caldera structure: results from analogue sandbox modeling. GSA Bulletin 116, 515–524.

Komuro, H., 1987. Experiments on cauldron formation: a polygonal cauldron and ring fractures. Journal of Volcanology and Geothermal Research 31, 139–149.

Komuro, H., Fujita, Y., Kodama, K., 1984. Numerical and experimental models on the formation mechanism of collapse basins during Green Tuff orogenesis of Japan. Bulletin of Volcanology 47, 649–666.

Lavallée, Y., Stix, J., Kennedy, B., Richer, M., Longpré, M.-A., 2004. Caldera subsidence in areas of variable topographic relief: results from analogue modeling. Journal of Volcanology and Geothermal Research 129, 219–236.

Lipman, P.W., 1984. The roots of ash flow calderas in western North America; windows into the tops of granitic batholiths. Journal of Geophysical Research 89B, 8801–8841.

Lipman, P.W., 1997. Subsidence of ash-flow calderas; relation to caldera size and magma-chamber geometry. Bulletin of Volcanology 59, 198–218.

Mandl, G., 1987. Tectonic deformation by rotating parallel faults: the bookshelf mechanism. Tectonophysics 141, 277–316.

Marrett, R.A., Allmendinger, R.W., Alonso, R.N., Drake, R.E., 1994. Late Cenozoic tectonic evolution of the Puna Plateau and adjacent foreland, NW Argentine Andes. Journal of South American Earth Sciences 7, 179–207.

Marti, J., Ablay, G.J., Redshaw, L.T., Sparks, R.S.J., 1994. Experimental studies of collapse calderas. Journal of the Geological Society (London) 151, 919–929.

McBirney, A.R., 1990. An historical note on the origin of calderas. Journal of Volcanology and Geothermal Research 42, 303–306.

Miller, G.F., 2001. The constraints on caldera alignment of Uranius Patera: regional tectonic stress vs. topographic gradient. Grosfils Research Letters 2, 17–20.

Moore, I., Kokelaar, P., 1998. Tectonically controlled piecemeal caldera collapse; a case study of Glencoe Volcano, Scotland. Geological Society of America Bulletin 110, 1448–1466.

Moos, D., Zoback, M.D., 1993. State of stress in the Long Valley caldera, California. Geology 21, 837–840.

Newhall, C.G., Dzurisin, D., 1988. Historical unrest at large calderas of the world. United States Geological Survey Bulletin 1855 (1108 pp.).

Orsi, G., De Vita, S., Di Vito, M., 1996. The restless, resurgent Campi Flegrei nested caldera (Italy): constraints on its evolution and configuration. Journal of Volcanology and Geothermal Research 74, 179–214.

Park, R.G., 1997. Foundations of structural geology, 3rd ed. Chapman and Hall, London.

Ramberg, H., 1981. Gravity, deformation and the Earth's crust, 2nd ed. Academic Press, London. 452 pp.

Roche, O., Druitt, T.H., 2001. Onset of caldera collapse during ignimbrite eruptions. Earth and Planetary Science Letters 191, 191–202.

Roche, O., Druitt, T.H., Merle, O., 2000. Experimental study of caldera formation. Journal of Geophysical Research 105, 395–416.

Seggiaro, R.E., Hongn, F.D., 1999. Tectonic influence in Cenozoic volcanism in North-Western Argentina. Acta Geologica Hispanica (now Geologica Acta) 34, 227–242.

Skilling, I.P., 1993. Incremental caldera collapse of Suswa volcano, Gregory Rift Valley, Keyna. Journal of the Geological Society (London) 150, 885–896.

Smith, R.L., Bailey, R.A., 1968. Resurgent cauldrons. Memoir-Geological Society of America, 613–662.

Troll, V.R., Emeleus, C.H., Donaldson, C.H., 2000. Caldera formation in the Rum Central igneous complex, Scotland. Bulletin of Volcanology 62, 301–317.

Troll, V.R., Walter, T.R., Schmincke, H.U., 2002. Cyclic caldera collapse: piston or piecemeal subsidence? Field and experimental evidence. Geology 30, 135–138.

Twiss, R.J., Moores, E.M., 1992. Structural geology, 1st ed. W. H. Freeman and Co. 532 pp.

van Wyk de Vries, B., Merle, O., 1996. The effect of volcanic constructs on rift fault patterns. Geology 24, 643–646.

van Wyk de Vries, B., Merle, O., 1998. Extension induced by volcanic loading in regional strike-slip zones. Geology 26, 983–986.

Wallmann, P.C., Pollard, D.D., Hildreth, W., Eichelberger, J.C., 1990. New structural limits on magma chamber locations at the Valley of Ten Thousand Smokes, Katmai National Park, Alaska. Geology 18, 1240–1243.

Walter, T.R., Troll, V.R., 2001. Formation of caldera periphery faults: an experimental study. Bulletin of Volcanology 63, 191–203.

Wilson, C.J.N., Houghton, B.F., McWilliams, M.O., Lanphere, M.A., Weaver, S.D., Briggs, R.M., 1995. Volcanic and structural evolution of Taupo Volcanic Zone, New Zealand: a review. Journal of Volcanology and Geothermal Research 68, 1–28.

Wolff, J.A., Gardner, J.N., 1995. Is the Valles Caldera entering a new cycle of activity? Geology 23, 411–414.